The Astrophysical Journal, 604:675–686, 2004 April 1

ANALYTIC FORMS OF THE PERPENDICULAR DIFFUSION COEFFICIENT IN MAGNETOSTATIC TURBULENCE

A. Shalchi, J. W. Bieber, and W. H. Matthaeus
Bartol Research Institute, University of Delaware, Newark, DE 19716
Received 2003 October 4; accepted 2003 December 17

ABSTRACT

Recently, a nonlinear theory for perpendicular diffusion of charged particles was presented. This theory is called the nonlinear guiding center theory and provides an integral equation for the perpendicular mean free path. In this paper we consider analytical solutions of this equation in the case of magnetostatic turbulence. The resulting formulas for the perpendicular mean free path are discussed. We also compare these new results with results of the quasi-linear theory for parallel diffusion and with observational results.

Subject headings: cosmic rays — diffusion — turbulence

1. INTRODUCTION

The scattering of energetic charged test particles in a turbulent electromagnetic field is a problem that is widely recognized to be of importance in space plasma physics and astrophysics (Jokipii 1966; Jokipii & Parker 1969; Jokipii, Kota, & Giacalone 1993; Jones, Jokipii, & Baring 1998). In the collisionless limit the interaction with the electromagnetic field takes the place of two-body Coulomb collisions as the principal scattering agent. Consequently, when a large-scale or mean magnetic field induces a preferred direction, diffusive transport, when it exists, differs in the parallel and perpendicular directions. For a variety of reasons, perpendicular transport, which is generally the weaker of the two effects, has also been the more difficult one to pin down at a theoretical level. The classical quasi-linear estimate, sometimes known as the field line random walk (FLRW) limit, concludes that the perpendicular diffusion coefficient is $\kappa_\perp = vD_\perp/3$, where v is the test particle velocity and $D_\perp$ is the Fokker-Planck (diffusion) coefficient associated with the random walk of static magnetic field lines. Though appealing, this result is known at this point to be generally incorrect, overestimating transport as a result of the secondary nonlinear influence of parallel scattering. The basic idea that parallel scattering suppresses perpendicular scattering has been around for some time, and various attempts to describe the net effect have been attempted, often in combinations with weak Coulomb scattering, shear, and dynamical effects.

To our knowledge it has only been through recent analytical and numerical work (Jokipii et al. 1993; Jones et al. 1998; Giacalone & Jokipii 1999; Kota & Jokipii 2000; Qin, Matthaeus, & Bieber 2002a, 2002b; Matthaeus et al. 2003) that the detailed understanding has begun to emerge the nature of the suppression and loss of perpendicular diffusion due to compound diffusive effects, and recovery of diffusion, in some cases. In particular, a promising theory for perpendicular diffusion known as the Nonlinear Guiding Center (NLGC) model has been described recently (Matthaeus et al. 2003). In the NLGC approach, particle gyrocenters are assumed to follow field lines, while experiencing parallel scattering. Diffusion in this case depends upon the randomization associated with dynamical effects, and sampling of the transverse spatial complexity of the turbulence. In direct comparison with numerical results extracted from ensembles of test particles, NLGC showed promise in accurately accounting for perpendicular diffusion for a range of parameters. Here we further elucidate some of the properties of the NLGC theory by examining its analytic solutions.

2. PERPENDICULAR MEAN FREE PATH IN MAGNETOSTATIC TURBULENCE

From the NLGC theory we obtain the following integral equation

$$\kappa_\perp = \frac{a^2 v^2}{3B_0^2} \int dk_x dk_y dk_z \frac{S(\boldsymbol{k})}{\frac{v}{\lambda_\parallel} + k_\perp^2 \kappa_\perp + k_\parallel^2 \kappa_\parallel + \gamma(\boldsymbol{k})}, \quad (1)$$

where we used $\kappa_\perp := \kappa_{xx} = \kappa_{yy}$ and $S := (S_{xx} + S_{yy})/2$. This equation follows from equation (7) of Matthaeus et al. (2003) for the case of axisymmetric turbulence. In equation (1) we used the numerical factor a, the particle velocity v, the magnetic background field B_0, the parallel mean free path $\lambda_\parallel$, the parallel spatial diffusion coefficient $\kappa_\parallel$, the damping function $\gamma(\boldsymbol{k})$, and the total power spectrum $S(\boldsymbol{k})$.

In the current paper we restrict our calculations to the case of magnetostatic turbulence

$$\gamma(\boldsymbol{k}) = 0, \quad (2)$$

and to the following power spectrum:

$$S(\boldsymbol{k}) = S^{2\mathrm{D}}(k_\perp)\delta(k_\parallel) + S^{\mathrm{slab}}(k_\parallel)\delta(\boldsymbol{k}_\perp), \quad (3)$$

with

$$S^{\mathrm{slab}} = C(\nu) l_{\mathrm{slab}} \delta B_{\mathrm{slab}}^2 (1 + k_\parallel^2 l_{\mathrm{slab}}^2)^{-\nu} \quad (4)$$

and

$$S^{2\mathrm{D}} = C(\nu) l_{2\mathrm{D}} \delta B_{2\mathrm{D}}^2 (1 + k_\perp^2 l_{2\mathrm{D}}^2)^{-\nu} \frac{1}{\pi k_\perp}, \quad (5)$$

where we used

$$C(\nu) = \frac{1}{2\sqrt{\pi}} \left[\Gamma(\nu)/\Gamma\left(\nu - \frac{1}{2}\right) \right]. \quad (6)$$

This function was chosen so that $\int d^3kS(\boldsymbol{k}) = \delta B^2/2$. Note that the parameter l_{slab} is related to the correlation length l_c through $l_{\mathrm{slab}} = l_c/[2\pi C(\nu)]$. Using the power spectrum defined through equations (3)–(6) we find for $\kappa_\perp$

$$\kappa_\perp = \frac{2a^2v^2}{3B_0^2}C(\nu)\left[l_{2\mathrm{D}}\delta B_{2\mathrm{D}}^2\int_0^\infty dk\frac{\left(1+k^2l_{2\mathrm{D}}^2\right)^{-\nu}}{\left(v/\lambda_\parallel\right)+k^2\kappa_\perp} + l_{\mathrm{slab}}\delta B_{\mathrm{slab}}^2\int_0^\infty dk\frac{\left(1+k^2l_{\mathrm{slab}}^2\right)^{-\nu}}{\left(v/\lambda_\parallel\right)+k^2\kappa_\parallel}\right]. \tag{7}$$

We can express the perpendicular mean free path,

$$\lambda_\perp = \frac{3}{v}\kappa_\perp, \tag{8}$$

and the parallel mean free path,

$$\lambda_\parallel = \frac{3}{v}\kappa_\parallel, \tag{9}$$

in terms of the spatial diffusion coefficients. Now we use the transformation $x = k\cdot l_{2\mathrm{D}}$ in the first integral and $x = k \cdot l_{\mathrm{slab}}$ in the second integral to obtain

$$\lambda_\perp = \frac{2a^2}{B_0^2}C(\nu)\left[\frac{3\delta B_{2\mathrm{D}}^2 l_{2\mathrm{D}}^2}{\lambda_\perp}\int_0^\infty dx\frac{\left(1+x^2\right)^{-\nu}}{\epsilon_{2\mathrm{D}}+x^2} + \frac{3\delta B_{\mathrm{slab}}^2 l_{\mathrm{slab}}^2}{\lambda_\parallel}\int_0^\infty dx\frac{\left(1+x^2\right)^{-\nu}}{\epsilon_{\mathrm{slab}}+x^2}\right]. \tag{10}$$

In equation (10) we introduced the dimensionless parameters

$$\epsilon_{2\mathrm{D}} = \frac{3l_{2\mathrm{D}}^2}{\lambda_\parallel\lambda_\perp} \tag{11}$$

and

$$\epsilon_{\mathrm{slab}} = \frac{3l_{\mathrm{slab}}^2}{\lambda_\parallel^2}. \tag{12}$$

In terms of the dimensionless function

$$I(\nu,\epsilon) = \int_0^\infty dx\frac{\left(1+x^2\right)^{-\nu}}{\epsilon+x^2}, \tag{13}$$

the perpendicular mean free path can be written as

$$\lambda_\perp = \frac{6a^2}{B_0^2}C(\nu)\left[\frac{l_{2\mathrm{D}}^2\delta B_{2\mathrm{D}}^2}{\lambda_\perp}I(\nu,\epsilon_{2\mathrm{D}}) + \frac{l_{\mathrm{slab}}^2\delta B_{\mathrm{slab}}^2}{\lambda_\parallel}I(\nu,\epsilon_{\mathrm{slab}})\right]. \tag{14}$$

To proceed with our calculations we have to analyze the function $I(\nu,\epsilon)$. This function can be expressed through a product of a β-function $B(x,y)$ and a hypergeometric function ${}_2F_1(a,b,c,x)$ (see Gradshteyn & Ryzhik 1966)

$$I(\nu,\epsilon) = \frac{1}{2\epsilon}B\left(\frac{1}{2},\frac{1}{2}+\nu\right){}_2F_1\left(1,\frac{1}{2},\nu+1,\frac{\epsilon-1}{\epsilon}\right). \tag{15}$$

With

$$B\left(\frac{1}{2},\frac{1}{2}+\nu\right) = \frac{\Gamma(1/2)\Gamma(\nu+1/2)}{\Gamma(\nu+1)} = \sqrt{\pi}\frac{\nu-1/2}{\nu}\frac{\Gamma(\nu-1/2)}{\Gamma(\nu)} \tag{16}$$

and with

$$F(\nu,\epsilon) \equiv {}_2F_1\left(1,\frac{1}{2},\nu+1,\frac{\epsilon-1}{\epsilon}\right), \tag{17}$$

we finally find

$$\frac{\lambda_\perp}{\lambda_\parallel} = \frac{2\nu-1}{4\nu}a^2\left[\frac{\delta B_{2\mathrm{D}}^2}{B_0^2}F(\nu,\epsilon_{2\mathrm{D}}) + \frac{\delta B_{\mathrm{slab}}^2}{B_0^2}F(\nu,\epsilon_{\mathrm{slab}})\right]. \tag{18}$$

This is still an exact, but nonlinear equation, because $\epsilon_{2\mathrm{D}}$ depends upon $\lambda_\perp$. In the next sections we consider analytical results of this equation for pure slab, pure two-dimensional, and composite geometry. One should note, however, that equation (18) can also be solved numerically.

3. THE PERPENDICULAR MEAN FREE PATH FOR PURE SLAB GEOMETRY

It should be noted that there are circumstances in which perpendicular transport in pure or nearly pure magnetostatic slab turbulence is subdiffusive—i.e., mean square perpendicular displacements increase more slowly than t^{+1}, where t is the time (Qin et al. 2002a; Kota & Jokipii 2000). Further, analytic theorems demonstrate that the perpendicular mean free path for a pure slab geometry must be zero since particles are tied to magnetic lines of force. In contrast, diffusive transport both parallel and perpendicular to the magnetic field is a central assumption of the NLGC theory, and thus this theory cannot accommodate subdiffusion. We speculate that the slab limit of the NLGC theory may apply in situations where slab modes dominate the turbulence energy, but there is nonetheless sufficient transverse structure in the field to permit diffusion to occur. To delve further into these issues is beyond the scope of the present work, but see Qin et al. (2002a) for a discussion of what might constitute "sufficient" transverse structure. In addition, the presence of dynamical effects may restore diffusion to pure slab geometries in a manner describable by the NLGC-theory. This possibility will be explored in future work. For the present we simply assume diffusion is recovered and proceed as follows.

In the case of pure slab geometry we have

$$\delta B_{2\mathrm{D}} = 0 \tag{19}$$

and

$$\delta B_{\mathrm{slab}} = \delta B. \tag{20}$$

In this special case equation (18) can be written as

$$\frac{\lambda_\perp}{\lambda_\parallel} = \frac{2\nu-1}{4\nu}a^2\frac{\delta B^2}{B_0^2}F(\nu,\epsilon_{\mathrm{slab}}). \tag{21}$$

This is an exact result for pure slab geometry. It is easy to see that in the pure slab case the perpendicular mean free path is only a function of ν, $\lambda_\parallel$, l_{slab}, δB, B_0, and of the parameter a.

For all values of these parameters we have

$$\lambda_\perp \sim \frac{\delta B^2}{B_0^2}. \tag{22}$$

In turn we consider two different cases for $\epsilon_{\rm slab}$. To do this it is necessary to know the asymptotic properties of the hypergeometric function. From Appendix A we know that

$$F(\nu, \epsilon) \approx \begin{cases} F_1(\nu) & \text{for } \epsilon \gg 1, \\ F_2(\nu)\sqrt{\epsilon} & \text{for } \epsilon \ll 1, \end{cases} \tag{23}$$

with the functions F_1 and F_2 defined as

$$F_1(\nu) \equiv \frac{2\nu}{2\nu - 1} \tag{24}$$

and

$$F_2(\nu) \equiv \sqrt{\pi}\,\frac{\Gamma(\nu+1)}{\Gamma(\nu+1/2)} = 2\pi C(\nu) F_1(\nu). \tag{25}$$

3.1. *The Case* $\lambda_\parallel \gg \sqrt{3}\, l_{\rm slab}$

In this case $\epsilon_{\rm slab}$ is a small number, and we find (see eq. [23])

$$\lambda_\perp \approx \sqrt{3}\frac{2\nu - 1}{4\nu} l_{\rm slab}\, F_2(\nu)\, a^2 \frac{\delta B^2}{B_0^2}. \tag{26}$$

Thus, in the case $\lambda_\parallel \gg \sqrt{3}\, l_{\rm slab}$, which is the normal case, the perpendicular mean free path is independent of the parallel mean free path and therefore independent of the rigidity. Note that equation (26) is very similar to the equations derived by Forman, Jokipii, & Owens (1974), Zank et al. (1998), and Le Roux, Zank, & Ptuskin (1999).

3.2. *The Case* $\lambda_\parallel \ll \sqrt{3}\, l_{\rm slab}$

In this case $\epsilon_{\rm slab}$ is a large number, and equation (21) becomes

$$\frac{\lambda_\perp}{\lambda_\parallel} \approx \frac{a^2}{2}\frac{\delta B^2}{B_0^2}. \tag{27}$$

3.3. *The Perpendicular Mean Free Path at* 1 AU

To compare our results with observations and simulations we have to specify the parameters. In the current paper we use values representative of the solar wind at 1 AU:

$$\begin{aligned} a^2 &= \frac{1}{3}, \\ \delta B &= B_0, \\ \nu &= \frac{5}{6}, \\ l_{\rm slab} &= 4.55 \times 10^9 \text{ m} \approx 0.030 \text{ AU}, \\ l_{\rm 2D} &= \frac{l_{\rm slab}}{10}. \end{aligned} \tag{28}$$

In the following discussions we always use this parameter set. If one or more parameters are different from equation (28), we note this. Using these parameters, Figure 1 compares the exact perpendicular mean free path (*dotted line*) with the analytic approximations derived above (*solid lines*).

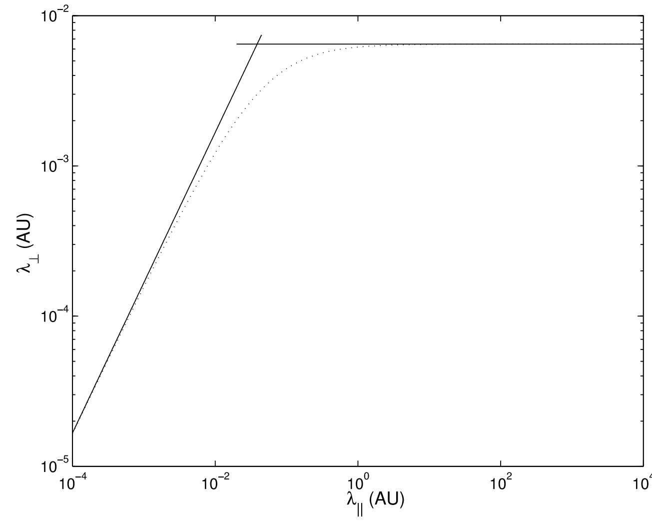

FIG. 1.—Perpendicular mean free path $\lambda_\perp$ as a function of the parallel mean free path $\lambda_\parallel$ for pure slab geometry. The dotted line shows the exact perpendicular mean free path computed numerically from eq. (18). The solid lines show the analytic approximations given by eqs. (26) and (27).

4. THE PERPENDICULAR MEAN FREE PATH FOR PURE TWO-DIMENSIONAL GEOMETRY

In this section we consider the case of pure two-dimensional geometry. It should be noted that the Jokipii et al. (1993) theorem on reduced dimensionality does not apply when the magnetic field coincides with the ignorable direction, as it does in pure two-dimensional turbulence.

To calculate the perpendicular mean free path as a function of rigidity with the NLGC theory, we need the parallel mean free path as a function of rigidity. In the current paper we use results of the quasi-linear theory (QLT) (see Appendix B). Therefore, it is questionable whether the case of pure two-dimensional geometry is useful in the pure magnetostatic turbulence, because here we have the QLT results, that $\lambda_\parallel^{\rm 2D} = \infty$ (see Shalchi & Schlickeiser 2004). But in the next section we demonstrate that in the case of composite geometry the two-dimensional contribution of the power spectrum dominates the perpendicular mean free path in most cases, which implies that the results of this section should be good approximations for the case of composite geometry. Further, in the case of medium or large amplitude two-dimensional turbulence, there is a nonlinear two-dimensional contribution to scattering, yielding a finite mean free path (Qin et al. 2002b).

In the case of pure two-dimensional geometry we have

$$\delta B_{\rm slab} = 0 \tag{29}$$

and

$$\delta B_{\rm 2D} = \delta B. \tag{30}$$

In this case equation (18) can be written as

$$\frac{\lambda_\perp}{\lambda_\parallel} = \frac{2\nu - 1}{4\nu} a^2 \frac{\delta B^2}{B_0^2}\, F(\nu, \epsilon_{\rm 2D}). \tag{31}$$

This is an exact result for pure two-dimensional geometry but equation (31) is a nonlinear equation. Therefore, we must consider two different cases for ϵ_{2D}.

4.1. *The Case* $\lambda_{\parallel}\, \lambda_{\perp} \ll 3\, l_{2D}^2$

In this case ϵ_{2D} is a large number, and we find together with equation (23)

$$\frac{\lambda_{\perp}}{\lambda_{\parallel}} \approx \frac{a^2}{2} \frac{\delta B^2}{B_0^2}. \tag{32}$$

This result corresponds precisely to the pure slab result of the last section in the limit of small $\lambda_{\parallel}$.

4.2. *The Case* $\lambda_{\parallel}\, \lambda_{\perp} \gg 3\, l_{2D}^2$

In this case ϵ_{2D} is a small number, and we find

$$\frac{\lambda_{\perp}}{\lambda_{\parallel}} \approx \frac{2\nu - 1}{4\nu}\, F_2(\nu)\, a^2 \frac{\delta B^2}{B_0^2}\, \sqrt{3} \frac{l_{2D}}{\sqrt{\lambda_{\parallel} \cdot \lambda_{\perp}}}, \tag{33}$$

where we used equation (23) again. Therefore, equation (33) can be written as

$$\lambda_{\perp} \approx \left[\frac{2\nu - 1}{4\nu}\, F_2(\nu)\, a^2 \frac{\delta B^2}{B_0^2}\, \sqrt{3}\, l_{2D}\right]^{2/3} \lambda_{\parallel}^{1/3}, \tag{34}$$

and we finally find

$$\lambda_{\perp} \sim \lambda_{\parallel}^{1/3}. \tag{35}$$

If we use dissipationless magnetostatic QLT results for $\lambda_{\parallel}$ (see Appendix B), we find for the rigidity dependence of the perpendicular mean free path

$$\begin{aligned} &\lambda_{\perp}(R \ll 1) \sim R^{1/9}, \\ &\lambda_{\perp}(R \gg 1) \sim R^{2/3}, \end{aligned} \tag{36}$$

where $R = R_L/l_{\rm slab}$. Note that for fixed field strength and bend-over scale $l_{\rm slab}$ the ratio R is proportional to the particle rigidity.

5. THE PERPENDICULAR MEAN FREE PATH FOR COMPOSITE SLAB/TWO-DIMENSIONAL GEOMETRY

In this section we consider the general case of composite geometry, which means that we have to consider both parts of equation (18). As in the two-dimensional case we must consider small and large values of ϵ_{2D} to solve the nonlinear equation.

5.1. *The Case* $\lambda_{\parallel}\, \lambda_{\perp} \ll 3\, l_{2D}^2$

In this case ϵ_{2D} is a large number, and we can use the approximation

$$F(\nu, \epsilon_{2D}) \approx F_1(\nu), \tag{37}$$

and we find the equation

$$\frac{\lambda_{\perp}}{\lambda_{\parallel}} \approx \frac{2\nu - 1}{4\nu} a^2 \left[\frac{\delta B_{2D}^2}{B_0^2} F_1(\nu) + \frac{\delta B_{\rm slab}^2}{B_0^2}\, F(\nu, \epsilon_{\rm slab})\right]. \tag{38}$$

The right side of this equation is only a function of $\lambda_{\parallel}$ and not of $\lambda_{\perp}$. Therefore, equation (38) is the final result of this subsection. For the function $F(\nu, \epsilon_{\rm slab})$ one can use the approximations presented before. In the case of $\lambda_{\parallel} \ll \sqrt{3}\, l_{\rm slab}$ we always find that the perpendicular mean free path is proportional to the parallel mean free path:

$$\frac{\lambda_{\perp}}{\lambda_{\parallel}} \approx \frac{a^2}{2} \frac{\delta B^2}{B_0^2}. \tag{39}$$

In the case that we have $\lambda_{\parallel} \gg \sqrt{3}\, l_{\rm slab}$, which should be satisfied for most cosmic rays at 1 AU we find

$$\frac{\lambda_{\perp}}{\lambda_{\parallel}} \approx \frac{2\nu - 1}{4\nu} a^2 \left[\frac{\delta B_{2D}^2}{B_0^2} F_1(\nu) + \frac{\delta B_{\rm slab}^2}{B_0^2}\, F_2(\nu) \sqrt{3} \frac{l_{\rm slab}}{\lambda_{\parallel}}\right]. \tag{40}$$

5.2. *The Case* $\lambda_{\parallel}\, \lambda_{\perp} \gg 3\, l_{2D}^2$

In this case ϵ_{2D} is a small number, and we can use

$$F(\nu, \epsilon_{2D}) \approx F_2(\nu) \sqrt{\epsilon_{2D}} = F_2(\nu) \sqrt{3}\, \frac{l_{2D}}{\sqrt{\lambda_{\parallel} \lambda \perp}} \tag{41}$$

to obtain

$$\frac{\lambda_{\perp}}{\lambda_{\parallel}} \approx \frac{2\nu - 1}{4\nu} a^2 \left[\frac{\delta B_{2D}^2}{B_0^2} F_2(\nu) \sqrt{3}\, \frac{l_{2D}}{\sqrt{\lambda_{\parallel} \lambda \perp}} + \frac{\delta B_{\rm slab}^2}{B_0^2}\, F(\nu, \epsilon_{\rm slab})\right], \tag{42}$$

which is a cubic equation for $\lambda_{\perp}^{1/2}$. This equation can be solved without using further approximations, as demonstrated in Appendix C. With the functions

$$\begin{aligned} q &= -\frac{2\nu - 1}{4\nu} a^2 \left(\frac{\delta B_{2D}}{B_0}\right)^2 F_2(\nu) \sqrt{3}\, l_{2D} \sqrt{\lambda_{\parallel}}, \\ p &= -\frac{2\nu - 1}{4\nu} a^2 \left(\frac{\delta B_{\rm slab}}{B_0}\right)^2 F(\nu, \epsilon_{\rm slab})\, \lambda_{\parallel}, \\ D &= \left(\frac{p}{3}\right)^3 + \left(\frac{q}{2}\right)^2, \end{aligned} \tag{43}$$

we find for the perpendicular mean free path

$$\lambda_{\perp} = \left[\left(-\frac{q}{2} + \sqrt{D}\right)^{1/3} + \left(-\frac{q}{2} - \sqrt{D}\right)^{1/3}\right]^2 \tag{44}$$

if $D \geq 0$ and

$$\lambda_{\perp} = \left(2 \sqrt{\frac{|\, p\, |}{3}} \cos\left\{\frac{1}{3} \arccos\left[-\frac{q}{2} (|\, p\, |/3)^{-3/2}\right]\right\}\right)^2 \tag{45}$$

if $D \leq 0$. The hypergeometric function in equation (43) can be approximated with equation (23) to simplify the results. In the important case of $\lambda_{\parallel} \gg \sqrt{3}\, l_{\rm slab}$ the hypergeometric functions can be well approximated through

$$F(\nu, \epsilon_{\rm slab}) \approx F_2(\nu) \sqrt{3} \frac{l_{\rm slab}}{\lambda_{\parallel}}. \tag{46}$$

In our further discussions we keep the hypergeometric function in the equations to obtain results with a higher precision.

5.3. *Comparison of the Analytical Approximations with Numerical Calculations*

Figure 2 shows the analytical approximations (eqs. [38], [44], and [45]) in comparison with numerical results. To obtain the numerical results we solved the nonlinear equation (18) numerically. The agreement is very good except the area where the condition $\lambda_\parallel \lambda_\perp \approx 3\, l_{2D}^2$ is fulfilled.

5.4. *The Asymptotic Properties of the Perpendicular Mean Free Path*

In this subsection we derive simple equations for $\lambda_\perp$ in the case of very small ($R \to 0$) and very high ($R \to \infty$) values of the parameter $R = R_l / l_{\rm slab}$, which is proportional to the rigidity.

5.4.1. $\lambda_\perp$ *in the Limit of Very Small Rigidities*

If the rigidity becomes small enough, we have $\lambda_\parallel \ll \sqrt{3} \cdot l_{\rm slab}$ and $\lambda_\parallel \lambda_\perp \ll 3\, l_{2D}^2$. In this case we always have

$$\frac{\lambda_\perp}{\lambda_\parallel} \approx \frac{a^2}{2} \frac{\delta B_{2D}^2}{B_0^2} \tag{47}$$

and therefore $\lambda_\perp \sim \lambda_\parallel \sim R^{1/3}$, where we used the QLT result $\lambda_\parallel(R \ll 1) \sim R^{1/3}$ (see Appendix B). It is important to note that this QLT results are only valid in the case of the power spectrum used in equation (B14) and in the case of magnetostatic turbulence. For a more realistic power spectrum with dissipation range and using the damping model of dynamical turbulence (both introduced by Bieber et al. 1994) the relations $\lambda_\parallel \approx \lambda_\parallel^{\rm slab}$ and $\lambda_\parallel^{\rm slab}(R \ll 1) \sim R^{1/3}$ are no longer valid (see Teufel & Schlickeiser 2002, 2003; Shalchi & Schlickeiser 2004).

5.4.2. $\lambda_\perp$ *in the Limit of Very High Rigidities*

In the case of $R \to \infty$, we assume $\lambda_\parallel \gg \sqrt{3}\, l_{\rm slab}$ and $\lambda_\parallel \lambda_\perp \gg 3\, l_{2D}^2$. In this case we can use equation (42), and the hypergeometric function can be approximated through

$$F(\nu, \epsilon_{\rm slab}) \approx F_2(\nu) \sqrt{3} \frac{l_{\rm slab}}{\lambda_\parallel}. \tag{48}$$

To proceed with our calculations we set $l_{2D} = l_{\rm slab}/10$ and assume that $\delta B_{\rm slab}^2 = (4/5)\, \delta B^2$ and $\delta B_{2D}^2 = (1/5)\, \delta B^2$. Under these assumptions equation (42) becomes

$$\lambda_\perp \approx \frac{2\nu - 1}{4\nu} a^2 F_2(\nu) l_{\rm slab} \frac{\delta B^2}{B_0^2} \frac{\sqrt{3}}{5} \left(\frac{2}{5} \sqrt{\frac{\lambda_\parallel}{\lambda_\perp}} + 1 \right). \tag{49}$$

Under the assumption that $\lambda_\perp \ll \lambda_\parallel$, we find that the two-dimensional contribution in the power spectrum controls the perpendicular mean free path, and we finally find

$$\lambda_\perp \approx \left[\frac{2\nu - 1}{4\nu} F_2(\nu) l_{\rm slab}\, a^2 \frac{\delta B^2}{B_0^2} \frac{2\sqrt{3}}{25} \right]^{2/3} \lambda_\parallel^{1/3}. \tag{50}$$

Employing the corresponding QLT result $\lambda_\parallel(R \gg 1) \sim R^2$ we find

$$\lambda_\perp(R \to \infty) \sim R^{2/3}. \tag{51}$$

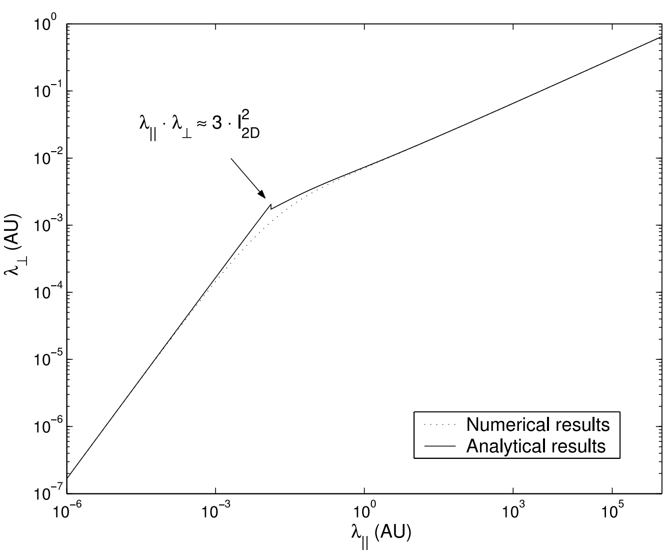

FIG. 2.—Solid line shows the perpendicular mean free path obtained from the analytical results (eqs. [38], [44], and [45]) in comparison with numerical results (*dotted line*). Results are for composite two-dimensional/slab geometry with the parameters given by eq. (28).

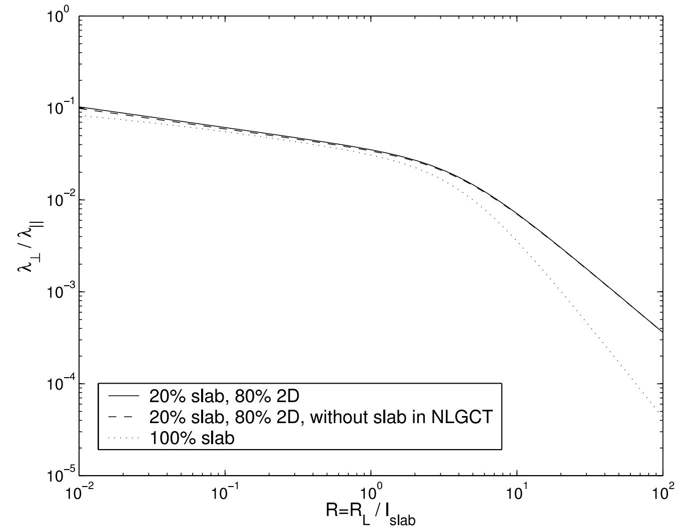

FIG. 3.—Ratio $\lambda_\perp/\lambda_\parallel$ for pure slab (*dotted line*) and composite (*solid line*) geometry. For calculating the dashed line we neglected the slab part of the NLGC theory to demonstrate that the perpendicular mean free path is controlled by the two-dimensional contribution. In this figure we used $l_{2D} = l_{\rm slab}$.

5.5. *The Perpendicular Mean Free Path for* 20% *Slab,* 80% *Two-dimensional, and* $l_{2D} = l_{\rm slab}/10$

As an example we consider the analytical results for the special case of

$$\delta B_{\rm slab}^2 = \frac{1}{5} \delta B^2,$$
$$\delta B_{2D}^2 = \frac{4}{5} \delta B^2,$$
$$l_{2D} = \frac{1}{10} l_{\rm slab} \tag{52}$$

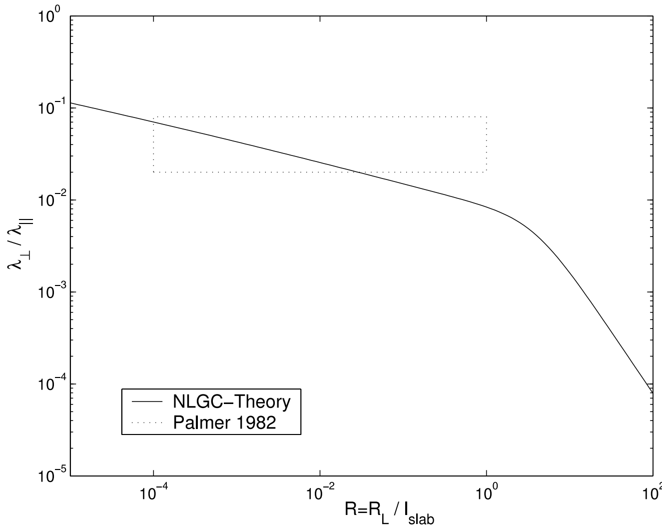

FIG. 4.—Ratio $\lambda_\perp/\lambda_\parallel$ for 80% two-dimensional/20% slab composite geometry in comparison to observations (*dotted box*; Palmer 1982). The theoretical curve assumes $l_{2\mathrm{D}} = 0.1\, l_{\mathrm{slab}}$.

to simplify the general results (eqs. [38], [44], and [45]). Using this parameter set we can consider the both cases for $\lambda_\perp \lambda_\parallel$ again.

5.5.1. *The Case* $\lambda_\perp \lambda_\parallel \ll 3\, l_{2\mathrm{D}}^2$

In this case we have

$$\frac{\lambda_\perp}{\lambda_\parallel} = \frac{2\nu - 1}{4\nu} a^2 \left(\frac{\delta B}{B_0}\right)^2 \left[\frac{4}{5}\, F_1(\nu) + \frac{1}{5}\, F(\nu, \epsilon_{\mathrm{slab}})\right]. \quad (53)$$

The maximum of the hypergeometric function is $F(\nu, \epsilon_{\mathrm{slab}}) = F_1(\nu)$ (see eq. [23]). Therefore, we can use the approximation

$$\frac{\lambda_\perp}{\lambda_\parallel} \approx \frac{2}{5}\, a^2\, \frac{\delta B^2}{B_0^2}. \quad (54)$$

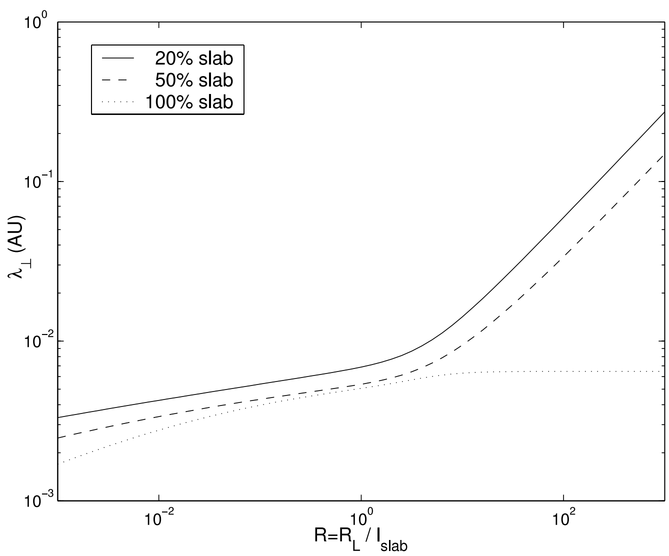

FIG. 5.—$\lambda_\perp$ for different $\delta B_{\mathrm{slab}}/\delta B_{2\mathrm{D}}$

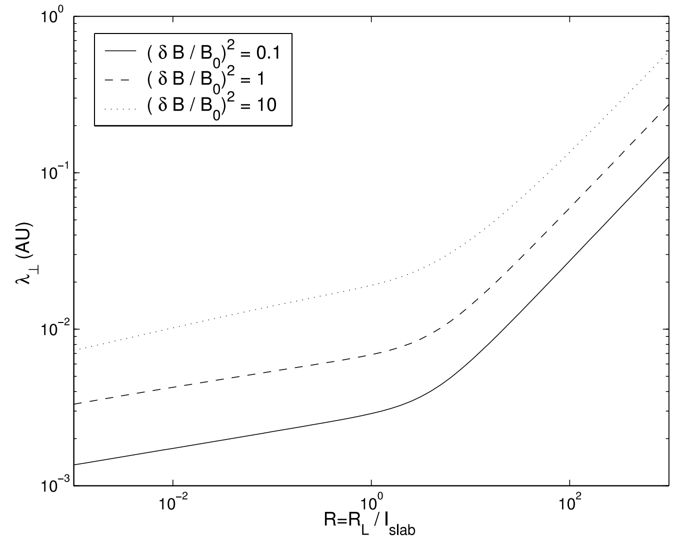

FIG. 6.—$\lambda_\perp$ for different $\delta B/B_0$

5.5.2. *The Case* $\lambda_\perp \lambda_\parallel \gg 3\, l_{2\mathrm{D}}^2$

To simplify the equations in this case we must consider the function D (see eq. [43]). If we do this we find that

$$D \approx \frac{q^2}{4} > 0. \quad (55)$$

Therefore, we obtain

$$\lambda_\perp \approx (-q)^{2/3} \approx \left[\frac{2\nu - 1}{5\nu} \sqrt{3} F_2(\nu) \frac{a^2}{10} \frac{\delta B^2}{B_0^2}\, l_{\mathrm{slab}}\right]^{2/3} \lambda_\parallel^{1/3}, \quad (56)$$

and we find

$$\lambda_\perp \sim \left(\frac{\delta B}{B_0}\right)^{4/3} l_{\mathrm{slab}}^{2/3}\, \lambda_\parallel^{1/3}. \quad (57)$$

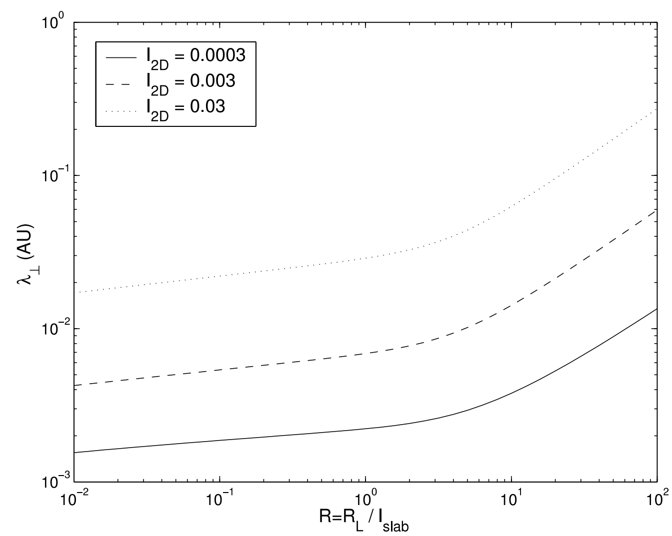

FIG. 7.—$\lambda_\perp$ for different $l_{2\mathrm{D}}$

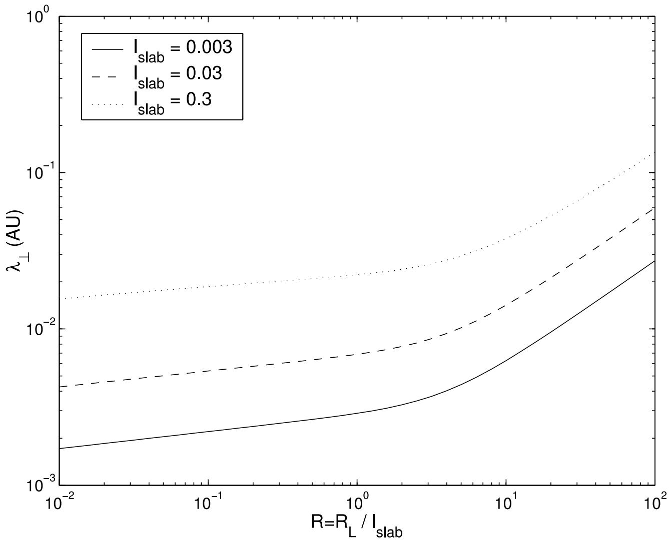

FIG. 8.—$\lambda_\perp$ for different l_{slab}

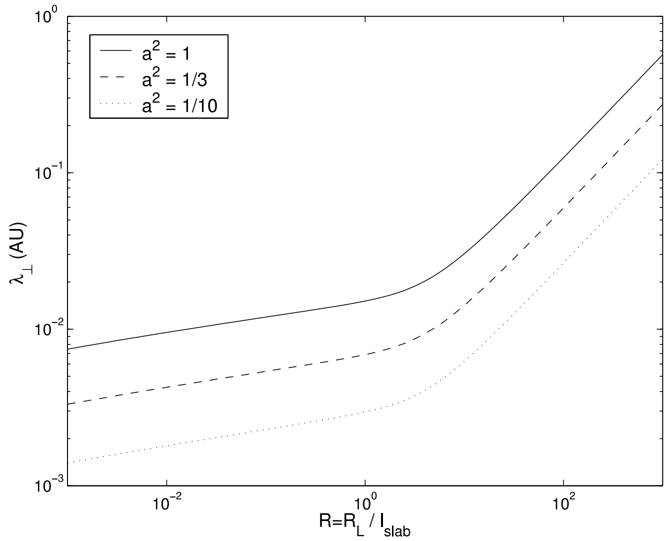

FIG. 10.—$\lambda_\perp$ for different a^2

Note that in both equations (54) and (56), the two-dimensional part of the power spectrum always controls the perpendicular mean free path.

5.6. *The Perpendicular Mean Free Path for Different Parameters*

In this subsection we calculate the perpendicular mean free path using the analytical results (eqs. [38], [44], and [45]) in the case of composite geometry. Figure 3 shows the ratio $\lambda_\perp/\lambda_\parallel$ as a function of $R = R_L/l_{\text{slab}}$, where we have again adopted the dissipationless magnetostatic QLT result for $\lambda_\parallel$. The dotted line in Figure 3 shows the pure slab case and the solid line shows the case of 20% slab and the 80% two-dimensional case. The dashed line shows also the 80% two-dimensional case, but here we neglected the slab contribution of the power spectrum in the NLGC theory. This means that in QLT the slab contribution controls the parallel mean free path, whereas the perpendicular mean free path is controlled by the two-dimensional contribution. Note, however, that the perpendicular mean free path is also controlled by the parallel mean free path and therefore the slab contribution is indirectly important for the perpendicular mean free path.

In Figure 4 we compare our results with observational results (Palmer 1982). A key result of this paper is that the NLGC theory can explain the Palmer observational results for the perpendicular mean free path if we set $l_{2\text{D}} = 0.1\, l_{\text{slab}}$.

To illustrate the influence of different parameters we calculated the perpendicular mean free path as a function of $R = R_L/l_{\text{slab}}$ for different values of $\delta B_{\text{slab}}/\delta B_{2\text{D}}$, B_0, $l_{2\text{D}}$, l_{slab}, ν, and a. Results appear in Figure 5, 6, 7, 8, 9, and 10. To obtain these results we employed the dissipationless magnetostatic QLT (see Appendix B) again.

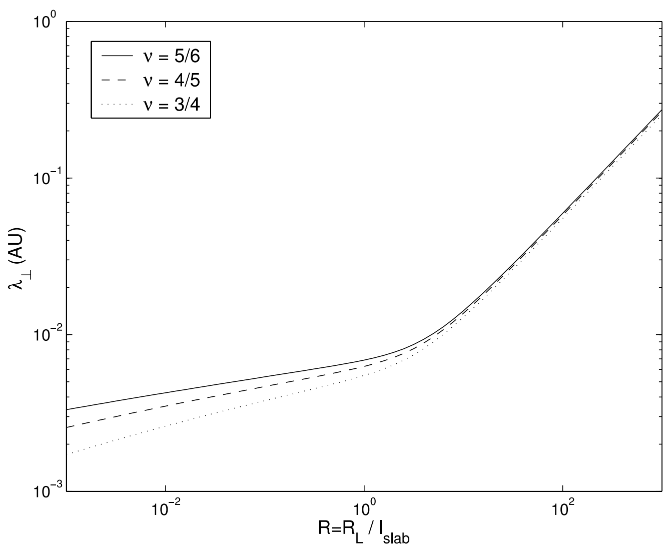

FIG. 9.—$\lambda_\perp$ for different ν

6. SUMMARY AND CONCLUSION

In this paper we derived analytical solutions of the NLGC theory that was presented by Matthaeus et al. (2003). We compared these new results with observational results from Palmer (1982). The agreement between the NLGC theory and simulations as well as observations is remarkable, suggesting the NLGC theory should find wide application in space physics and astrophysics.

The derived equations for the perpendicular mean free path provide a wide range of applications. One important application is to use the analytical results to calculate initial values for the numerical calculations of $\lambda_\perp$. This will reduce the calculation time enormously.

Our derived analytical results for composite geometry (see eqs. [38], [44], and [45]) are very general. In contrast to other analytical results (e.g., Zank et al. 2004) the results derived here can be applied also for all possible combinations of the governing parameters ϵ_{slab} and $\epsilon_{2\text{D}}$ (eqs. [11] and [12]).

This work profited enormously from discussions at the Potchefstroom International Cosmic Ray Workshop in 2002 March and the Bochum International Cosmic Ray Workshop in 2003 March. This research was supported by the National Science Foundation under grant ATM-0000315.

APPENDIX A

ASYMPTOTIC PROPERTIES OF THE FUNCTION $F(\nu, \epsilon)$

In the current paper we have to calculate the asymptotic properties of the function

$$F(\nu, \epsilon) = {}_2F_1\left(1, \frac{1}{2}, \nu + 1, \frac{\epsilon - 1}{\epsilon}\right). \tag{A1}$$

To do this we approximate the hypergeometric function for large and small ϵ in turn.

A1. THE CASE $\epsilon \gg 1$

In the case of large ϵ the function $F(\nu, \epsilon)$ can be approximated through

$$F(\nu, \epsilon \gg 1) \approx {}_2F_1\left(1, \frac{1}{2}, \nu + 1, 1\right). \tag{A2}$$

Using the well-known equation

$${}_2F_1(a, b; c; 1) = \frac{\Gamma(c)\Gamma(c - a - b)}{\Gamma(c - a)\Gamma(c - b)} \tag{A3}$$

if $c > a + b$, we find

$$F(\nu, \epsilon \gg 1) \approx \frac{\Gamma(\nu + 1)\Gamma(\nu - 1/2)}{\Gamma(\nu)\Gamma(\nu + 1/2)} = \frac{2\nu}{2\nu - 1} \equiv F_1(\nu). \tag{A4}$$

Note that our calculations are only valid in the case of $\nu > 1/2$.

A2. THE CASE $\epsilon \ll 1$

In this case we have to transform the hypergeometric function. To do this we can use

$${}_2F_1(a, b; c; z) = (1 - z)^{-b}\, {}_2F_1\left(b, c - a, c, \frac{z}{z - 1}\right), \tag{A5}$$

and the function $F(\nu, \epsilon)$ can be written as

$$F(\nu, \epsilon) = \sqrt{\epsilon}\, {}_2F_1\left(\frac{1}{2}, \nu, \nu + 1, 1 - \epsilon\right), \tag{A6}$$

which can be approximated through

$$\begin{aligned} F(\nu, \epsilon \ll 1) &\approx \sqrt{\epsilon}\, {}_2F_1\left(\frac{1}{2}, \nu, \nu + 1, 1\right) \\ &= \sqrt{\epsilon}\sqrt{\pi}\frac{\Gamma(\nu + 1)}{\Gamma(\nu + 1/2)} \\ &\equiv \sqrt{\epsilon}\, F_2(\nu). \end{aligned} \tag{A7}$$

APPENDIX B

QLT RESULTS FOR THE PARALLEL MEAN FREE PATH

In order to determine the rigidity dependence of the perpendicular mean free path with the NLGC theory we need analytical expressions for the parallel mean free path. In this paper we use results of the quasi-linear theory (QLT) in the case of dissipationless magnetostatic turbulence. As shown in Shalchi & Schlickeiser (2004), the two-dimensional contribution to the parallel mean free path is equal to zero in the case of magnetostatic turbulence in the quasi-linear limit. To calculate the parallel mean free path we use the same formalism as presented in Bieber et al. (1994):

$$\lambda_\parallel = \frac{3v}{2}\int_0^1 d\mu \frac{(1-\mu^2)^2}{\Phi(\mu)}. \tag{B1}$$

In equation (B1) we introduced the Fokker-Planck coefficient

$$\Phi = \frac{\Omega^2}{B_0^2}(1-\mu^2)\int_{-\infty}^{+\infty} dk_z\, S_{\rm slab}(k_z) D(k_z), \tag{B2}$$

with the power spectrum $S_{\rm slab}(k_z)$ and the resonance function $D(k_z)$, which is related to the dynamical correlation function $\Gamma(k_z, t)$ (Bieber et al. 1994) by

$$D(k_z) = {\rm Re}\int_{-\infty}^{+\infty} dt\, e^{i(k_z\mu v - \Omega)t}\Gamma(k_z, t). \tag{B3}$$

In the magnetostatic limit $\Gamma = 1$ this function becomes

$$D(k_z) = \frac{2\pi}{v \mid \mu \mid}\delta\left(k_z - \frac{\Omega}{\mid \mu \mid v}\right). \tag{B4}$$

With this result we find

$$\Phi = \frac{2\pi\Omega^2}{v \mid \mu \mid B_0^2}(1-\mu^2) S_{\rm slab}\left(k_z = \frac{1}{R_L \mid \mu \mid}\right). \tag{B5}$$

For the power spectrum we use

$$S_{\rm slab} = C(\nu)\, l_{\rm slab}\delta B_{\rm slab}^2 (1 + l_{\rm slab}^2 k^2)^{-\nu}, \tag{B6}$$

and we obtain for the Fokker-Planck coefficient

$$\Phi(\mu) = \frac{2\pi C(\nu) v}{R^2 l_{\rm slab}}\frac{\delta B^2}{B_0^2}\,(1-\mu^2)\,\mu^{2\nu-1}\left(\mu^2 + R^{-2}\right)^{-\nu}, \tag{B7}$$

where we introduced the parameter

$$R \equiv \frac{R_L}{l_{\rm slab}} = \frac{v}{\Omega\, l_{\rm slab}}. \tag{B8}$$

Therefore, we find for the parallel mean free path

$$\lambda_\parallel = \frac{3}{4\pi C(\nu)}\, l_{\rm slab}\, \frac{B_0^2}{\delta B^2}\, R^2\, K(\nu, R). \tag{B9}$$

In the last equation we introduced the integral $K(\nu, R)$

$$K(\nu, R) = \int_0^1 d\mu\left(\mu^{1-2\nu} - \mu^{3-2\nu}\right)\left(\mu^2 + R^{-2}\right)^{\nu}. \tag{B10}$$

This integral can be expressed through hypergeometric functions

$$\begin{aligned} K(\nu, R) = &\frac{R^{-2\nu}}{2}\left[\frac{1}{1-\nu}\,{}_2F_1\left(1-\nu, -\nu, 2-\nu, -R^2\right)\right] \\ &- \left[\frac{1}{2-\nu}\,{}_2F_1\left(2-\nu, -\nu, 3-\nu, -R^2\right)\right]. \end{aligned} \tag{B11}$$

The function $K(\nu, R)$ can also be expressed through elementary functions if we consider large and small values of the parameter R:

$$K(\nu, R) \approx \begin{cases} \dfrac{R^{-2\nu}}{2(1-\nu)(2-\nu)} & \text{for } R \ll 1, \\ \dfrac{1}{4} & \text{for } R \gg 1. \end{cases} \tag{B12}$$

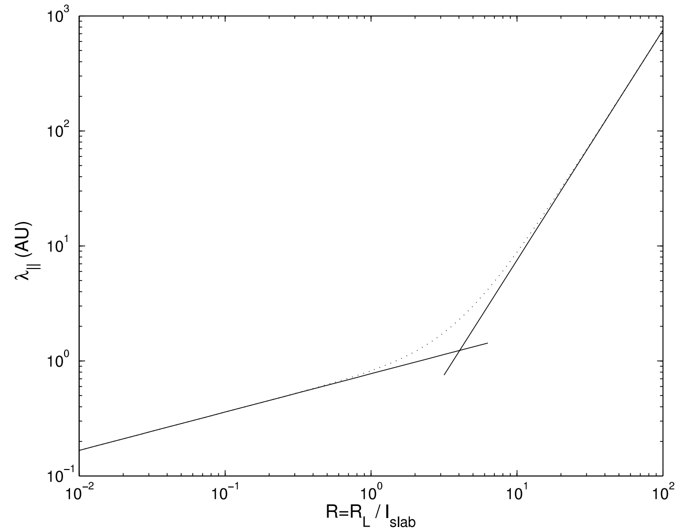

FIG. 11.—Parallel mean free path for 20% slab and 80% two-dimensional in the dissipationless magnetostatic limit calculated with QLT. The dotted line shows the exact result, the solid lines show the approximations.

With the results above the parallel mean free path can be written as

$$\lambda_{\|} = \frac{3\, l_{\rm slab}}{8\pi C(\nu)} \left(\frac{B_0}{\delta B_{\rm slab}}\right)^2 R^{2-2\nu} \left[\frac{1}{1-\nu_2} F_1\left(1-\nu, -\nu, 2-\nu, -R^2\right) - \frac{1}{2-\nu}\, {}_2F_1\left(2-\nu, -\nu, 3-\nu, -R^2\right)\right], \tag{B13}$$

which is the exact QLT result in the dissipationless magnetostatic limit. For the case $R \ll 1$ we find

$$\lambda_{\|}(R \ll 1) \approx \frac{3\, l_{\rm slab}}{8\pi C(\nu)} \left(\frac{B_0}{\delta B_{\rm slab}}\right)^2 \frac{R^{2-2\nu}}{(1-\nu)(2-\nu)}, \tag{B14}$$

and in the case $R \gg 1$ we have

$$\lambda_{\|}(R \gg 1) \approx \frac{3\, l_{\rm slab}}{8\pi C(\nu)} \left(\frac{B_0}{\delta B_{\rm slab}}\right)^2 \frac{R^2}{2}. \tag{B15}$$

In Figure 11 we have shown the exact QLT result (eq. [B13]) and the approximations (eqs. [B14] and [B15]). To do this we used the following set of parameters:

$$\begin{aligned} \delta B &= B_0, \\ \nu &= \frac{5}{6}, \\ l_{\rm slab} &= 4.55 \times 10^9 \text{ m} \approx 0.030 \text{ AU}, \\ \delta B_{\rm slab}^2 &= 0.2\, \delta B^2. \end{aligned} \tag{B16}$$

To obtain more realistic expressions for the parallel mean free path we refer to Teufel & Schlickeiser (2002, 2003), where a similar formalism was used to derive equations for $\lambda_{\|}$ including a dissipation range in the power spectrum. Those papers also considered two different functions for Γ: the damping model of dynamical turbulence and the random sweeping model.

APPENDIX C

SOLVING THE CUBIC EQUATION FOR THE PERPENDICULAR MEAN FREE PATH

In the case $\lambda_{\|}\, \lambda_{\perp} \gg 3 l_{\rm 2D}^2$ and assuming composite geometry, the perpendicular mean free path can be written as

$$\frac{\lambda_{\perp}}{\lambda_{\|}} \approx \frac{2\nu - 1}{4\nu} a^2 \left[\frac{\delta B_{\rm 2D}^2}{B_0^2} F_2(\nu) \sqrt{3}\, \frac{l_{\rm 2D}}{\sqrt{\lambda_{\|} \lambda \perp}} + \frac{\delta B_{\rm slab}^2}{B_0^2} F(\nu, \epsilon_{\rm slab})\right]. \tag{C1}$$

Now we can use

$$
\begin{aligned}
x &\equiv \sqrt{\lambda_\perp}, \\
q &\equiv -\frac{2\nu-1}{4\nu} a^2 \left(\frac{\delta B_{2\mathrm{D}}}{B_0}\right)^2 F_2(\nu)\sqrt{3}\, l_{2\mathrm{D}} \sqrt{\lambda_\parallel}, \\
p &\equiv -\frac{2\nu-1}{4\nu} a^2 \left(\frac{\delta B_{\mathrm{slab}}}{B_0}\right)^2 F(\nu, \epsilon_{\mathrm{slab}})\, \lambda_\parallel, \\
D &\equiv \left(\frac{p}{3}\right)^3 + \left(\frac{q}{2}\right)^2
\end{aligned}
\tag{C2}
$$

to rewrite equation (C1) as

$$
x^3 + px + q = 0, \tag{C3}
$$

which is a cubic equation in x. To solve this equation we must consider three different cases for D.

C1. THE CASE $D > 0$

In this case we have the three solutions:

$$
\begin{aligned}
x_1 &= \alpha_1 + \alpha_2, \\
x_2 &= -\frac{\alpha_1 + \alpha_2}{2} + \sqrt{3}\frac{\alpha_1 - \alpha_2}{2} i, \\
x_3 &= -\frac{\alpha_1 + \alpha_2}{2} - \sqrt{3}\frac{\alpha_1 - \alpha_2}{2} i,
\end{aligned}
\tag{C4}
$$

where we used

$$
\alpha_1 = \left(-\frac{q}{2} + \sqrt{D}\right)^{1/3} \tag{C5}
$$

and

$$
\alpha_2 = \left(-\frac{q}{2} - \sqrt{D}\right)^{1/3}. \tag{C6}
$$

x must be a real number, which implies that only x_1 is a physical solution of the cubic equation.

C2. THE CASE $D < 0$

In this case we have also three solutions:

$$
\begin{aligned}
x_1 &= +2\sqrt{\frac{|\,p\,|}{3}} \cos\left(\frac{\beta_1}{3}\right), \\
x_2 &= -2\sqrt{\frac{|\,p\,|}{3}} \cos\left(\frac{\beta_1 - \pi}{3}\right), \\
x_3 &= -2\sqrt{\frac{|\,p\,|}{3}} \cos\left(\frac{\beta_1 + \pi}{3}\right),
\end{aligned}
\tag{C7}
$$

where we used

$$
\cos(\beta_1) = -\frac{q}{2}(|\,p\,|/3)^{-3/2}. \tag{C8}
$$

The solutions x_2 and x_3 are negative numbers. Therefore, only x_1 is again a physical solution.

C3. THE CASE $D = 0$

In the last case we have $D = 0$ and we can use equation (C4) or equation (C7), because in this case we have $\alpha_1 = \alpha_2$ and $\cos(\beta_1) = 1$. Therefore, x_1 in equation (C4) and x_1 in equation (C7) are equal. The solutions x_2 and x_3 are always negative numbers. Therefore, we find for x the two physical solutions:

$$x = \alpha_1 + \alpha_2 \tag{C9}$$

if $D \geq 0$, and

$$x = 2\sqrt{\frac{|\,p\,|}{3}}\cos\left(\frac{\beta_1}{3}\right) \tag{C10}$$

if $D \leq 0$.

REFERENCES

Bieber, J. W., et al. 1994, ApJ, 420, 294
Forman, M. A., Jokipii, J. R., & Owens, A. J. 1974, ApJ, 192, 535
Giacalone, J., & Jokipii, J. R. 1999, ApJ, 520, 204
Gradshteyn, I. S., & Ryzhik, I. M. 1966, Table of Integrals, Series, and Products (New York: Academic Press)
Jokipii, J. R. 1966, ApJ, 146, 480
Jokipii, J. R., Kota, J., & Giacalone, J. 1993, Geophys. Res. Lett., 20, 1759
Jokipii, J. R., & Parker, E. N. 1969, ApJ, 155, 777
Jones, F. C., Jokipii, J. R., & Baring, M. G. 1998, ApJ, 509, 238
Kota, J., & Jokipii, J. R. 2000, ApJ, 531, 1067
Le Roux, J. A., Zank, G. P., & Ptuskin, V. S. 1999, J. Geophys. Res., 104, 24845
Matthaeus, W. H., et al. 2003, ApJ, 590, L53
Palmer, I. D. 1982, Rev. Geophys. Space Phys., 20, 335
Qin, G., Matthaeus, W. H., & Bieber, J. W. 2002a, Geophys. Res. Lett., 29, 7
———. 2002b, ApJ, 578, L117
Shalchi, A., & Schlickeiser, R. 2004, ApJ, in press
Teufel, A., & Schlickeiser, R. 2002, A&A, 393, 703
———. 2003, A&A, 397, 15
Zank, G. P., et al. 1998, J. Geophys. Res., 103, 2085
———. 2004, J. Geophys. Res., submitted